Journal of Heat and Mass Transfer Research

Journal homepage: http://jhmtr.semnan.ac.ir

Semnan University

Modeling the Transient Absorption of Particulate Drugs in the Human Upper Airways

Reza Tabe [a], Roohollah Rafee [*,a], Mohammad Sadegh Valipour [a], Goodarz Ahmadi [b]

[a] *Faculty of Mechanical Engineering, Semnan University, Semnan, Iran.*

[b] *Department of Mechanical and Aeronautical Engineering, Clarkson University, Potsdam, NY, USA.*

PAPER INFO

Paper history:

Recieved: 2020-07-25

Revised: 2020-12-15

Accepted: 2020-12-19

Keywords:

Particle absorption;
Human Upper Airway;
Oral Inhalation;
CFPD;
Drug delivery.

ABSTRACT

Predicting the dynamics of aerosols in the respiratory tract is crucial for the analysis of toxic effects of particulate matters and to the respiratory targeted drug delivery. The present work focuses on evaluating the transient absorption of drug particles on the airway walls of the respiratory tract. For this purpose, simulations of airflow and particulate matters inside a three-dimensional model of respiratory airways were coupled to a one-dimensional drug absorption model. The drug absorption from mucus to the respiratory walls was studied using the transient mass transfer equations in a multilayer model. Different breathing rates of 5, 7.5, and 10 Lit/min were considered in the simulations. Particles with different sizes of 2, 5, 10, and 30μm were released at the entrance of the oral cavity during the inspiration phase. The airflow velocity distribution, particle concentration, and flux of drugs at the interface of mucus-tissue were studied in detail. The transient absorption process that occurred over the breathing time considered of 4 s was evaluated. The results showed that the drug mass flow rate at the mucus-tissue interface and the drug concentration in the tissue layer decreases with time. Also, it was found that after inspiration, the location of the maximum concentration changes from mucus to the tissue layer.

DOI: 10.22075/jhmtr.2020.20957.1295

1. Introduction

Airflow in the respiratory airways could be laminar, transitional, or turbulent, depending on the breathing rate and geometry of the airway passages. Because of the complex geometry, it is difficult to define a critical Reynolds number for the human airway. It has been controversial to determine the airflow regime inside the upper airway of the human. Earlier investigations [1-3], suggested that the airflow in the upper airways is laminar for the breathing rates below 15L/min.

Recently, there have been several studies on computational modeling of the transport and deposition of airborne particles in various passages, including human airways. Wang et al. [4], Srivastav et al. [5], and Hemmati [6] analyzed the particle deposition near the wall, concluding that the flow Reynolds number, duct walls, and particle size play significant roles in near-wall particle deposition. Further investigations on aerosols in different geometries have been done by Mirzaee et al. [7], and Hamedi Estakhrsar et al. [8]. These studies highlight the role of impaction efficiencies for laminar and turbulent viscous flows and how more bends cause a significant increase in the pressure drop. Zamankhan et al. [9], Shanley et al. [10], Ghahramani et al. [11], and Ghalati et al. [12] have studied micro and nanoparticle deposition in the respiratory system routes computationally. Despite the anatomical differences of the human subjects used in these studies, the simulation results were in qualitative agreement with the experimental data. Nikookar et al. [13] were investigated targeted drug delivery with the application of magnetic particles. Their results indicated a great improvement in the drug deposition in the presence of a magnetic field. Some prior investigations were making airflow simulations for simplified respiratory passages that did not fit the actual status [16-18]. In other related works realistic geometries of the path were used [19-20]. Abouali et al. [14] investigated the effect of

[*] *Corresponding Author: Roohollah Rafee, Faculty of Mechanical Engineering, Semnan University, Semnan, Iran.*
Email: rafee@semnan.ac.ir

virtual endoscopic surgery, while in [15], the accuracy of the continuous and discrete random walk stochastic models for simulation of inertial and Brownian particles was studied. Also, the effect of unsteady breathing on particle transport and deposition was evaluated in the study of Naseri et al. [3]. Recently, Shang et al. [21] reported the presence of secondary flow patterns in the larynx-trachea segment and left main bronchus. Also, the maximum pressure drop of 60, and 350 Pascal was reported for the flow rates of 18, and 50L/min, respectively. Haghnegahdar et al. [22] developed a model of computational fluid-particle dynamics (CFPD) plus host cell dynamics, which predicts the deposition and transport of the influenza A virus. They presented quantitative results that can be used for finding the essential mechanisms of lower and upper route infections.

One of the important and challenging areas of study is the assessment and management of the inhaled airborne particles in the respiratory system. These particles are released from various sources of contamination or therapeutic such as toxic environmental pollutants, combustion products, drug delivery, etc. In both cases, particle deposition in the respiratory tract is determined by computational fluid and particle dynamics (CFPD) methods. The Discrete Phase Model of the Fluent software has some errors for turbulent dispersion of the particles. These errors are mainly due to the miscalculations of the velocity fluctuations in turbulent gas flow near the walls [6]. However, in the laminar flow, there are no such errors. On the other hand, the errors of turbulent dispersion of the particles are also available in the OpenFOAM software. In the study of Greifzu et al. [23] two benchmark problems were investigated. Their results showed that the particle dispersion is slightly under-predicted when ANSYS FLUENT is used, whereas OpenFOAM overestimates the dispersion. On the other hand, therefore, using different software has its own advantages and disadvantages. Completion of calculations precisely after deposition of the particles onto a surface wall is a limitation for gas-particle models because, after the deposition of the particles, their fate is not available. One of the new issues facing the researchers is a study of drug penetration in mucous and tissue layers when the spray of drug inhaled. It is necessary to make a coupling between CFPD simulations and the models of drug penetration inside the mucous and tissues, i.e. these models integrate with existing CFPD simulations [24].

Cohen-Hubal et al. [25] utilized the mass transfer resistance in the nasal lining (wall boundary) to evaluate the ozone dosimetry in a rat nasal passage. They discovered that the mucus resistance was significant for explaining the amount and location of ozone uptake and mucosa thickness may play a role in the resulting pattern of ozone-induced harm. Keyhani et al. [26] used a mass transfer boundary condition on the nasal cavity wall, which included the influence of solubility and diffusivity of odorants on the mucosal lining and the thickness of the mucus layer. Their data suggested that the particle absorption occurs under a nearly quasi-steady-state process. Contrary to the assumption of steady-state absorption in earlier investigations, Tian and Longest [27] found that during the respiratory cycle transient wall absorption occurs. They assumed that at the air-mucus interface, the vapor concentration was constant. The results showed that for the nasal model, the difference between the steady and transient absorption is quite significant for compounds with high and medium solubility. Tian and Longest [28] developed a transient absorption model for toxic vapors, which was coupled to the simulation of the air-vapor transport in the respiratory tract. The particle mass flux at the air-mucus interface was considered as a function of its concentration in the air-phase. Their results showed that transient absorption was significantly different from the steady-state predictions.

In this paper, the transient absorption of the particulate drugs on the airway wall of the respiratory tract was investigated at different breathing rates. For this purpose, a 3-D realistic model of respiratory airways (from the oral cavity to the end of the trachea) was coupled to a 1-D absorption model of the medicine. This type of coupling was not previously done for particulate drugs in the literature. To validate the computational method, the results were compared with the earlier experimental and computational data in the literature. In the previous studies, the unsteady absorption of the particles was not simulated. However, in the present paper, the absorption process was simulated by solving a system of transient equations. In addition, the airflow velocity contours, concentration profiles of the particles, and the drug mass flux were evaluated numerically and discussed.

2. Method

2.1. Oral-Trachea Airway and Multilayer Model of Wall

In this study, images of the upper airways from lips to the end of the trachea (including oral cavity, pharynx, larynx, and trachea) taken from the computed axial tomography scan of a healthy non-smoking 32-year-old male are used in constructing the 3D model for the present computational and experimental studies. The transient absorption of particles in a multilayer system of the airway wall, including air, mucus, tissue, and blood layers, as shown in Figure 1, was considered. The transient absorption process via the airway wall included the diffusion into the mucus and tissue, which needed three partition coefficients and two diffusion coefficients to describe in a multilayer model [29]. Generally, as an inhaled particle is deposited, it has only two fates: (a) it is removed via mucociliary clearance, or (b) it is absorbed

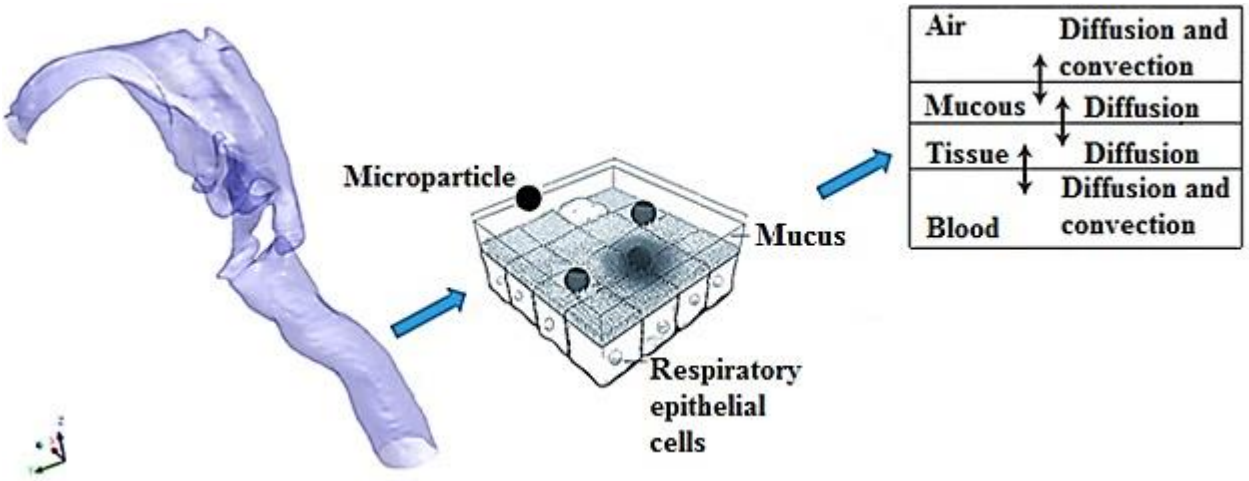

Figure 1. Schematic of a realistic respiratory tract model integrated with the multi-compartment wall unit.

across the epithelial barrier. Various absorption mechanisms have been demonstrated for pulmonary drug substances, including (a) transporter-mediated absorption and efflux (b) passive diffusion (c) internalization into immune cells, and (d) vesicle-mediated endocytosis [30]. Lipophilic particles easily diffuse across the cellular membranes, while hydrophilic medicines cross mostly via extracellular routes, such as intercellular junction pores or by active transport. The thickness of each layer was based on the described values for the respiratory airway, including the nasal cavity, throat, larynx, and mouth [31]. In this region, the reported thicknesses are about 15 and 50 μm, respectively, for mucus and tissue layers [28, 31]. In the present study, the Mometasone furoate (MF) is used as a therapeutic drug. This medicine usually used in the management of nasal inflammation, dermatoses and the treatment of bronchial asthma [32].

2.2. Chemical properties

Based on the study of Hayduk and Laudie [33, 34], the mucus diffusion coefficient for this drug is $D_{mucus} = 4.3 \times 10^{-6}\, cm^2/s$ [32]. The diffusion coefficient of the species into the tissue is assumed to be approximately one-third of its value in water [35-36]. The air-mucus partition coefficient is defined as [29]:

$$\lambda_{ma} = \frac{C_m}{C_a} \quad (1)$$

where on air-mucus side C_m and C_a are the species concentrations in the mucus and air with units of gr/cm^3. It should be noted that the values of C_a are obtained from the particle deposition profile on the mucus surface by the CFD simulation of the gas-particle flow. For this purpose, the maximum amount of particle deposition on the wall, i.e., at hotspot points, was obtained by particle tracking. In fact, the ANSYS Fluent software searches the surfaces of the wall boundary cells at which the maximum deposition occurs. We named these surfaces as hotspots. For different airflow rates and particle diameters the values of C_a are given in Table 1. Generally, the size of aerosol medicines created from commercial inhalers differs from 0.1 to 60μm and are poly-disperse, which results in their deposition in several areas of the respiratory system [30].

Table 1. Values of MF concentration in the air side of the mucus-air interface (gr/cm^3).

	Particle Diameter			
Flow rate (L/min)	**2 μm**	**5 μm**	**10 μm**	**30 μm**
5	0.0018	0.0039	0.0048	0.041
7.5	0.0012	0.0028	0.0089	0.057
10	0.0027	0.0078	0.0072	0.017

For small particles, the maximum concentration on the wall increases with the flow rate, i.e. higher flow rates gave higher maximum concentration. This is not the case for the larger particles. That is, the location of the hot spot and distribution of the deposited particles over the walls varies with the particle size. Also, species with $\lambda_{ma} > 1$ in the mucus layer are considered highly soluble, and $\lambda_{ma} = 1$ will be known as intermediate solubility. For most species, the tissue-blood partition coefficient is assumed to be equal to the unit [37]. The mucus-tissue partition coefficient can be obtained as [34]:

$$\lambda_{tm} = \frac{1}{\lambda_{bt}} \frac{\lambda_{ba}}{\lambda_{ma}} \quad (2)$$

where λ_{bt} and λ_{ba} are the tissue-blood and air-blood partition coefficients, respectively. According to various studies, the physical properties of the MF are reported in Table 2.

2.3. Governing Equations

As noted before, generally, for breathing rates less than 15 L/min, the regime of the airflow is laminar. The governing equations for airflow in their incompressible form are given a

Table2. Values of transport parameters for MF.

Parameter	Symbol	Value
Species diffusivity in mucus [32]	D_{mucus}	$4.3 \times 10^{-6}\, cm^2/s$
Species diffusivity in tissue [35]	D_{tissue}	$1.43 \times 10^{-6}\, cm^2/s$
Tissue-mucus partition coefficient [33]	λ_{tm}	1
Mucus-air partition coefficient [37]	λ_{ma}	1

Mass conservation

$$\frac{\partial u_i}{\partial x_i} = 0 \tag{3}$$

Momentum balance

$$\frac{\partial u_i}{\partial t} + u_j \frac{\partial u_i}{\partial x_j} = -\frac{1}{\rho}\frac{\partial p}{\partial x_i} + \frac{\mu}{\rho}\frac{\partial^2 u_i}{\partial x_j \partial x_j} \tag{4}$$

where u_i is the velocity, p is the pressure, ρ is the air density, and μ is the dynamic molecular viscosity. Assuming no chemical reactions and convection in the mucus and tissue layers, the rate of mass concentration absorbed into the mucus and the tissue is obtained by solving the following transient diffusion equation system:

$$\frac{\partial C_m(y,t)}{\partial t} = D_m \frac{\partial^2 C_m(y,t)}{\partial y^2}, y \in [0, H_m] \tag{5}$$

$$\frac{\partial C_t(y,t)}{\partial t} = D_t \frac{\partial^2 C_t(y,t)}{\partial y^2}, y \in [H_m, H_m + H_t] \tag{6}$$

where t is the time variable, and the y-direction is the depth in the mucus and tissue layers (Figure 2). Here D_m and D_t are chemical species diffusion coefficients, respectively, in the mucus and tissue layer. They are assumed to be constant in both layers.

Parameters H_m and H_t are mucus and tissue thickness in a specific area of the airway route, respectively. The concentrations of a chemical species in the mucus and the tissue layers given, respectively, by $C_m(y,t)$ and $C_t(y,t)$ vary with the time and space. Initially, the concentration of the drug in the mucus and tissue is assumed to be zero. The boundary conditions are:

$$C_m(y,t)_{|y=0} = \lambda_{ma} C_a(y,t)_{|y=0} \tag{7}$$

$$C_t(y,t)_{|y=H_m} = \lambda_{tm} C_m(y,t)_{|y=H_m} \tag{8}$$

$$-D_m \frac{\partial C_m(y,t)}{\partial y}_{|y=H_m} = -D_t \frac{\partial C_t(y,t)}{\partial y}_{|y=H_m} \tag{9}$$

$$C_t(y,t)_{|y=H_m+H_t} = 0 \tag{10}$$

The assumption is at the blood level the concentration is zero as the blood is going to wash it away. λ_{ma} and λ_{tm} are the air-mucus and mucus-tissue partition coefficients, respectively. $C_a(y,t)$ is obtained by CFD simulation (Table 1). Because breathing includes 2 seconds of inspiration and 2 seconds of exhalation, in the present study, the value of $C_a(y,t)$ is assumed to be zero after 2 seconds (There is no deposition during exhalation).

2.4. Solution method

The ANSYS-FLUENT (v18) software, which uses the finite volume method, was used to solve the airflow governing equations. The second-order upwind scheme was used to discretize the convective terms. For pressure-velocity coupling, the SIMPLE algorithm was used. The pressure boundary condition is used at the inlet of the model, and the no-slip boundary condition is imposed at the passage walls. Mass flow outlet boundary condition is used at the exit of the airway model. The oral-trachea model was meshed by ANSYS-ICEM software. Details of the generated mesh were described by Tabe et al. [19]. Because extra-thoracic airways have irregular geometries, a hybrid unstructured tetrahedral mesh was generated in the bulk of the domain while near the mucus, there are seven layers of fine prismatic cells. The primary width of the prismatic cells adjacent to the wall is 0.05 mm, and it amplifies normal to surface with the expansion ratio of 1.2. A sample grid cross-section in an axial plane is shown in Figure 3. Five several grids with 0.8, 1.2, 4.4, 7.6, and 9.7 million cells were created to study the grid independency of the solution. The results for velocity profiles in the oropharynx and trachea regions showed that the differences between the results of the grid with 7.6 million cells are the same as those for the grid with 9.7 million cells. Therefore, the grid with 7.6 million elements was selected for the subsequent computational analysis.For checking the validity of numerical simulation, the obtained numerical results are compared with the data in the literature. The tracking and deposition of particles and their absorption are evaluated for the pipe geometries of the experimental study of Pui et al. [38]. Figure 4 shows the simulation results for the case of fully developed pipe flow with two internal diameters of 3.95 and 8.50 mm at Reynolds number of 1000 versus the Stokes number (St) defined as

$$St = C\rho_p U D_p^2 / 18\mu r \tag{11}$$

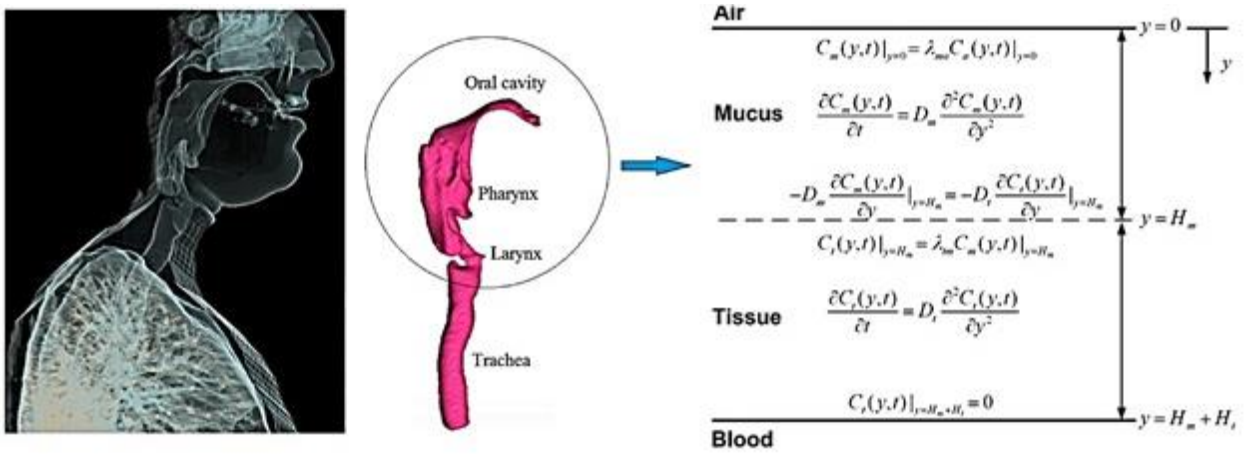

Figure 2. Air, mucus, tissue, and blood (AMTB) and system setup for numerical solutions.

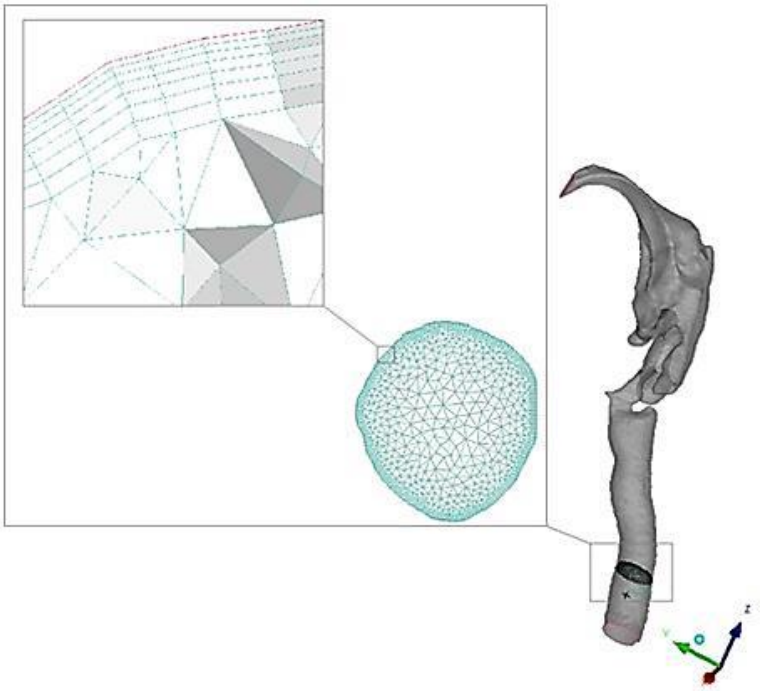

Figure 3. Sample section of the computational mesh and mesh arrangement near the wall.

Table3. Values of maximum differences between the CFD simulation and experimental data

	i.e. 3.95mm	i.e. 8.50 mm
Stokes number	0.32	0.2
Maximum diff.	7%	11%

Here C is the slip correction factor, ρ_p is the density of the particle, U is mean axial fluid velocity, D_p is the particle diameter, $\mu$is the viscosity, and r is the tube radius. The Stokes number (non-dimensional relaxation time) is a measure of inertia effects. Figure 4 shows good agreement between the present model predictions and the experimental data of Pui et al. [38] and assures the accuracy of the numerical results. The maximum values of the differences are listed in Table 3.

An in-house developed FORTRAN code was used to solve the transient diffusion equation system. The governing equations for the multilayer model (Eqs. (5) to (10)) were discretized using a finite difference method. The implicit method was used for the transient term, and the central discretization method was used for the diffusion term. Three different grids with 24, 32, and 42 nodes were considered for the grid independence study of transient diffusion code. The simulation results for MF concentration at t=2 and 3 s for different grids are shown in Figure 5. It is seen that the differences between the results of the grid of case 1 (5 nodes in mucus and 19 nodes in tissue) are the same as those for the grids of case 2 (7 nodes in mucus and 25 nodes in tissue) and case 3 (11 nodes in mucus and 31 nodes in tissue). Therefore, the grid of case 1 was selected for the subsequent computational analysis.

To verify the developed code, its predictions were compared with the results of Tian & Longest [28] in Figure 6. The concentration values at the mucus and tissue interface indicate the effect of the mucus–tissue partition coefficient. These results are for acetaldehyde vapor, which has devastating effects on the respiratory tract [39]. A point-by-point comparison between the present simulations and the previous results of [28] shows very good agreement with the maximum difference of about 1%.

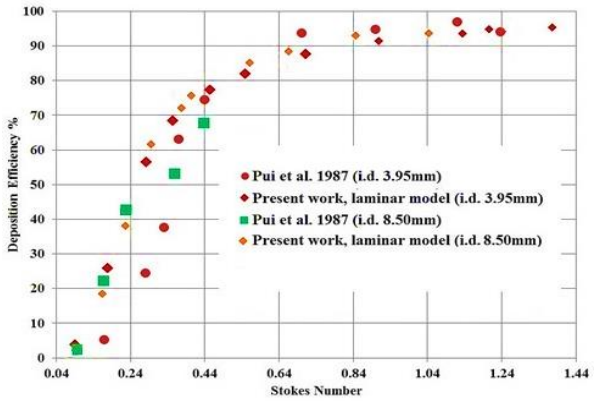

Figure 4. Validation of CFD simulation by comparing the present work with the experimental study of Pui et al. [38].

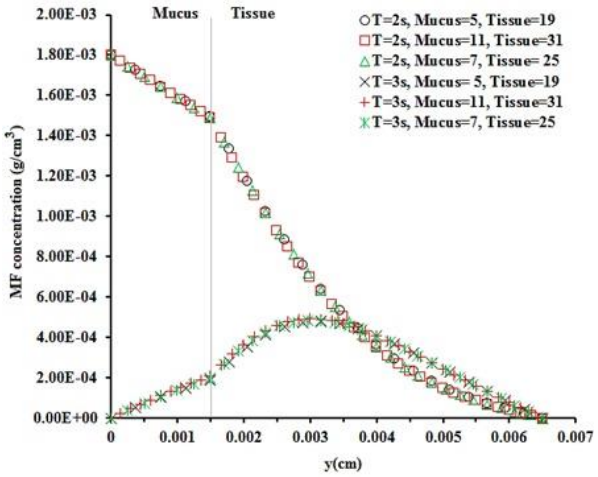

Figure 5. Grid independency test results for transient diffusion of MF in mucus and tissue

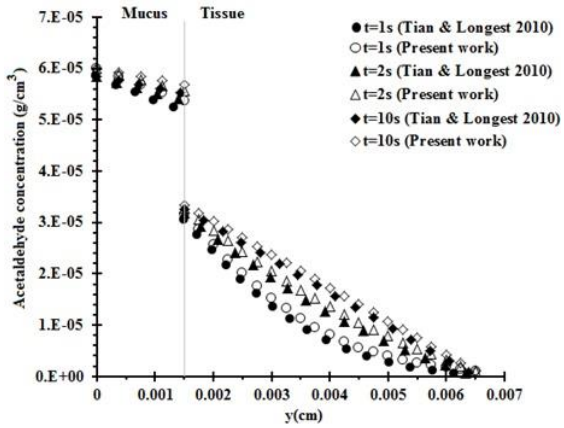

Figure 6. Validation of solution by comparing the present work with Tian & Longest [28] for acetaldehyde vapor in the mucus and tissue layers.

3. Results and discussion

Figure 7 depicts the velocity counters for three different breathing rates of 5, 7.5, and 10 L/min in the oropharynx, laryngopharynx, and a part of the trachea region. Airflow enters uniformly into the oral cavity and then experiences an expansion from the end of the hard palate to the oropharynx, leading to rather complicated structures in this region. It is seen due to the variation in the flow direction in the oropharynx, a higher airflow velocity occurs near the outer wall. As the breathing rate increases, more complicated airflow patterns are observed. Figure 7 shows an expansion in the airflow passage after the oropharynx region. Also, a high-velocity airflow field, the so-called laryngeal jet, in the laryngopharynx region is observed. The maximum velocities at the laryngeal jet for different breathing rates of 5, 7.5, and 10 L/min are, respectively, 4.23, 8.54, and 11.86 m/s..

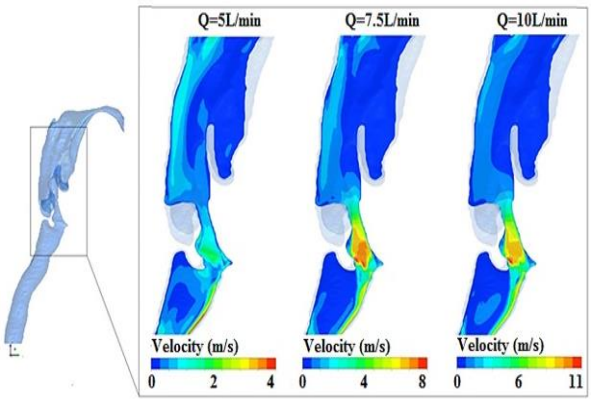

Figure 7. Velocity counters for three inspiration flow rates of 5, 7.5, and 10 L/min in the oropharynx, laryngopharynx, and a part of the trachea region.

Concentration profiles (g/cm3) for Mometasone furoate (MF) within the air-mucus-tissue- blood system are shown in Figures 8, 9, and 10 respectively, for particles with diameters of 2, 5, and 30 µm. In each of these figures, the time evolution of the concentration profiles at t=0.5, 1, 1.5, 2, 2.5, and 3 s are plotted. Concentration values in mucus and tissue indicate the temporal nature of the absorption process. In each case, the concentration curves for $t \leq 2$ s indicate that the maximum values of concentration occur in the mucus layer. In contrast, for higher time (t>2s), the peak values occur in the tissue layer. Concentration values at the mucus-tissue interface are affected by the magnitude of the partition coefficient. As expected, these figures show that the concentration values in the mucus layer are higher than those in the tissue. This type of transport from high concentration to low concentration (Passive diffusion) of particulate drugs, from the airway into the sub mucosa can happen thru the intercellular junctions between the pulmonary epithelial cells or via the epithelial cells [40].

Figure 8 shows the concentration profiles for the 2-µm particles. It is seen that the concentration of MF for the breathing rate of 7.5 L/min is lowest compared to the cases for the breathing rate of 5 and 10 L/min. The difference in the concentration profiles for the airflow rates of 5, 7.5, and 10 L/min was the result of the difference in the value of C_a (Table 1). It should be noted that the key parameters in drug absorption are the shape, particle size, charge, transporter substrate, metabolic stability, molecular polar surface area, lipophilicity, percentage of polar area in the total molecular surface, and hydrogen bonding potential [30]. These discrepancies in C_a values over time will result in a variable rate of absorption and flux into the AMTB model. As can be seen, at t=0.5 s, for all three flow rates, most of the medicine is located in the mucus layer. Over time, at the end of the inspiration phase, i.e., t=2 s the medicine spreads into the mucus and tissue layers. Similar results were reported for benzene and acetaldehyde by Tian and Longest [27, 28].

Figure 9 shows the variations of concentration with time for the 5 µm particles are almost the same as those found in the 2 µm particles. The obtained results for 2 and 5 μm particles show that the transient diffusion occurs similarly for different particle sizes over the studied period of time. As can be seen, as the final stage of breathing approaches, that is exhalation, the accumulation of the medicine in the mucus layer decreases, and the peak concentration locations move to the tissue layer. Such behavior is seen in the membrane transporters in drug distribution into the lung tissues and in the absorption of inhaled medicines into the systemic circulation. Experimental investigations have demonstrated the role of the membrane transporters on the pharmacodynamics, pharmacokinetic, and safety profiles of many inhaled medicines. Also, drug transporters in the lung can mediate the uptake of medicines from the systemic circulation into the lung tissue, resulting in amplified pulmonary drug accumulation, which carries therapeutic advantages in the etiology of lung dysfunctions, like asthma and chronic obstructive pulmonary disease (COPD) [41]. The reduction in the peak value of the concentration occurs due to the absorption of the medicine by the blood. Also, at the time t=3 s, the amount of peak MF concentration decreases. By examining the obtained results, it can be seen that at the same air flow rate, the transient time increases as the particle diameter gets larger.

For 30 µm particles, Figure 10 shows that the initial concentration values are nearly one order of magnitude larger compared with the previous cases for smaller particles. It occurs because of the higher deposition of the larger particles at the entrance route. Also, by the same postulation, more deposition occurs at higher flow rates, i.e. the transient peak values of airflow rates of 5 and 7.5 L/min are lower than that of 10 L/min. The particle size considerably affects the deposition location inside the respiratory route. Particles smaller than 3µm are deposited in the deep lungs where the maximum absorption into the systemic circulation happens. Also, small particles have greatly dissolution rates. Furthermore, particle size influences the rate of phagocytosis by alveolar macrophages, which is likely the most notable clearance passage of slowly dissolving medicines from the deep lungs. Alveolar macrophages efficiently phagocytosis particles with a diameter range of 0.5–5µm, which is the optimal size range for alveolar deposition, resulting in systemic bioavailability and a noteworthy reduction in the alveolar residence time [42, 43]. One of the benefits of delivering high concentrations of the drug directly to the illness area is the reduction of systemic side-effects [44]. In addition, sluggish mucociliary clearance in the lung results in prolonged residence in the lung environment [45]. It should be noted that these analyzes can contribute to the effectiveness of the drug in many lung diseases since it gives us the maximum concentration of the medicine during inhalation of the patient.

Figure 11 presents the concentration variations with time for different particle sizes at a flow rate of 10 L/min. As shown, for the times less than 0.5s the concentration in

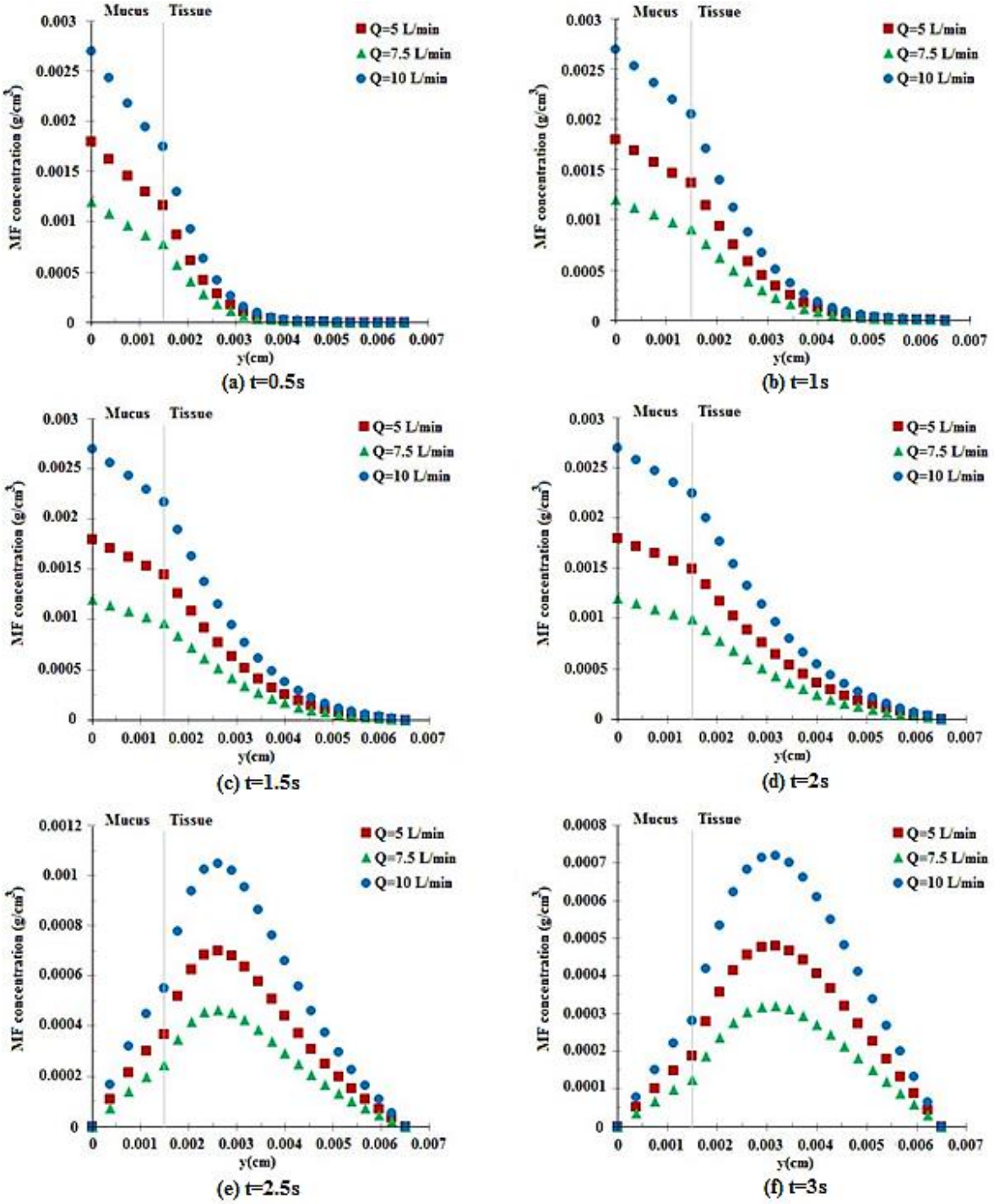

Figure 8. Concentration values in the AMTB system for 2 μm particles.

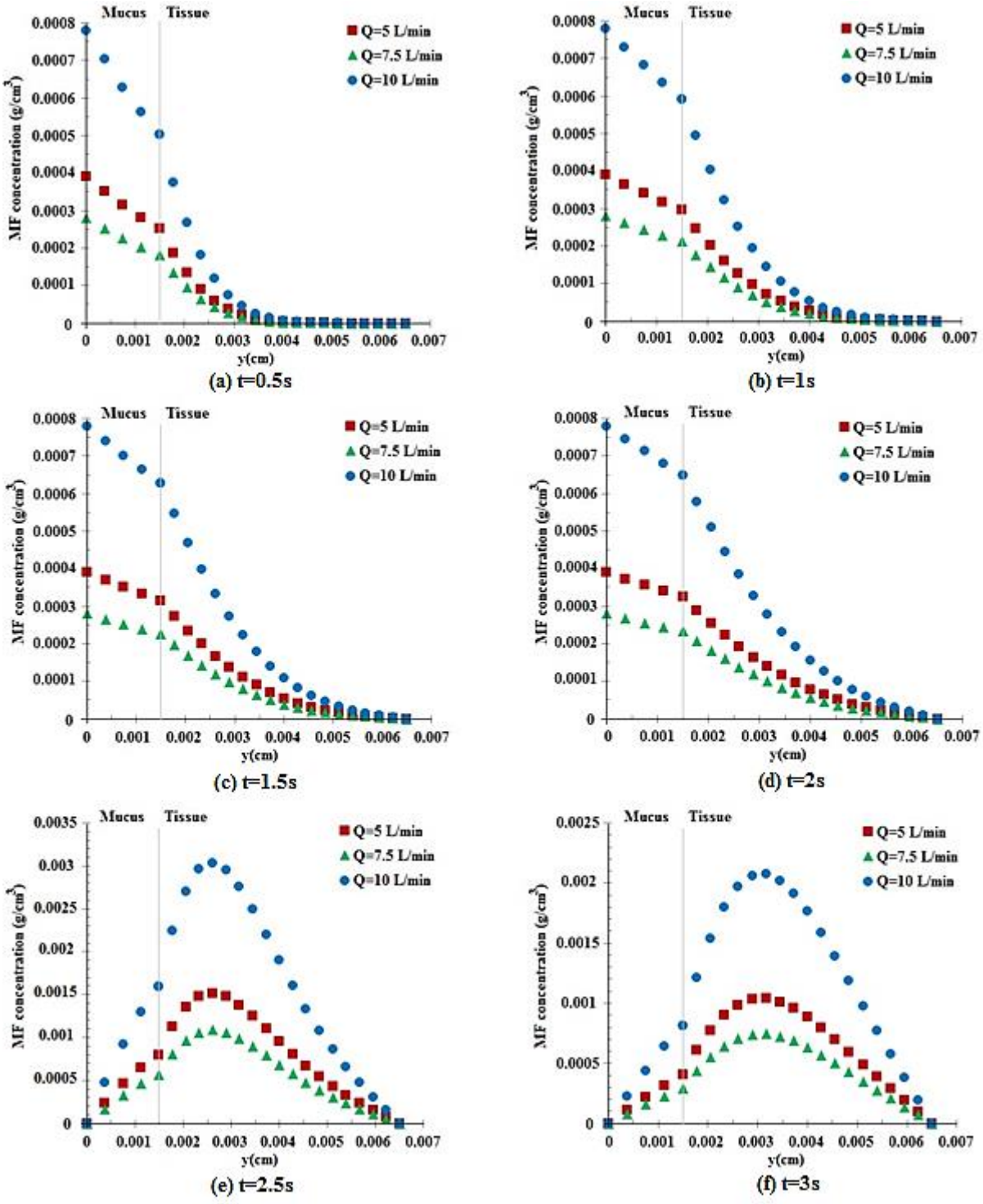

Figure 9. Concentration values in the AMTB system for 5 μm particles.

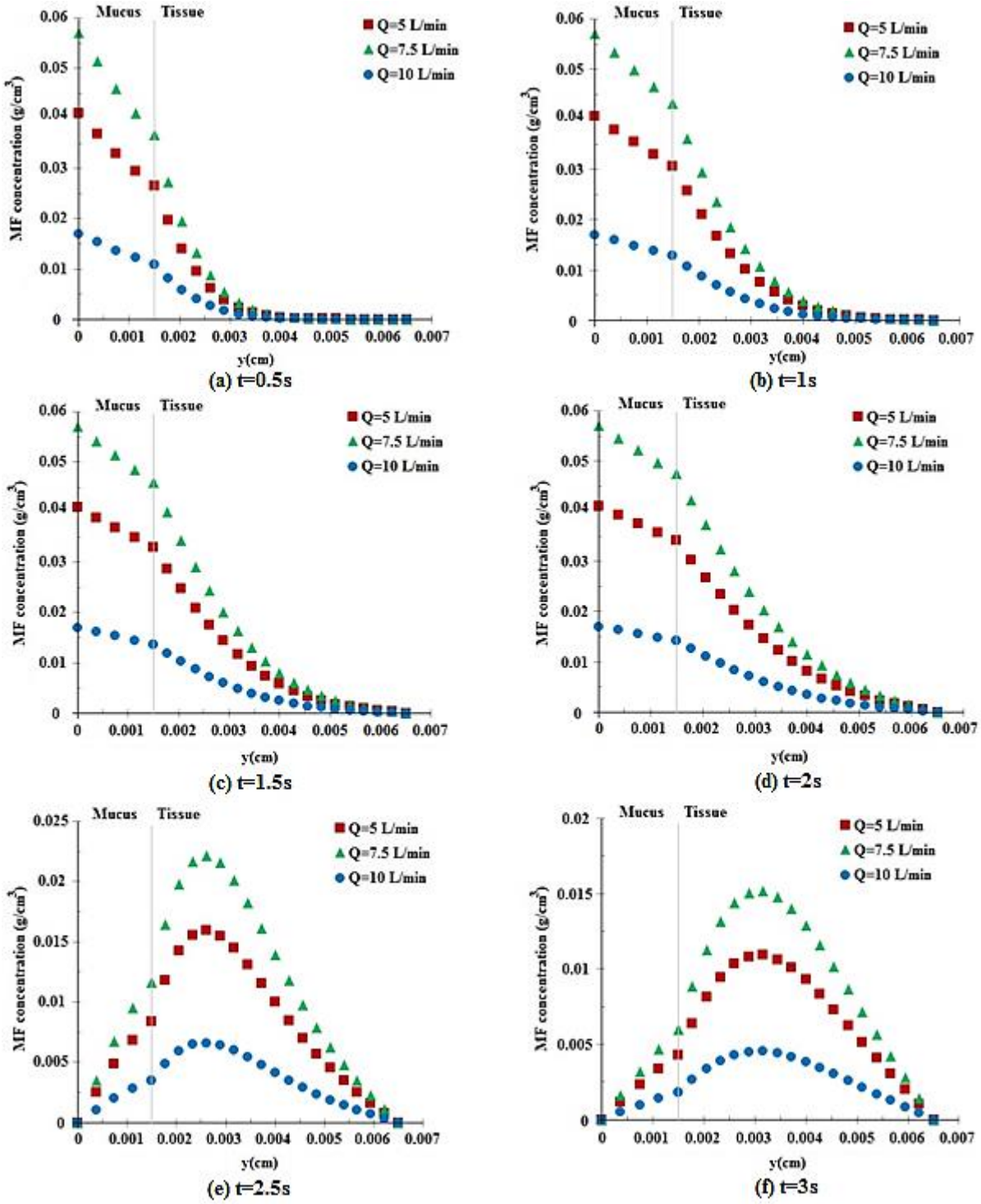

Figure 10. Concentration values in the AMTB system for 30 μm particles.

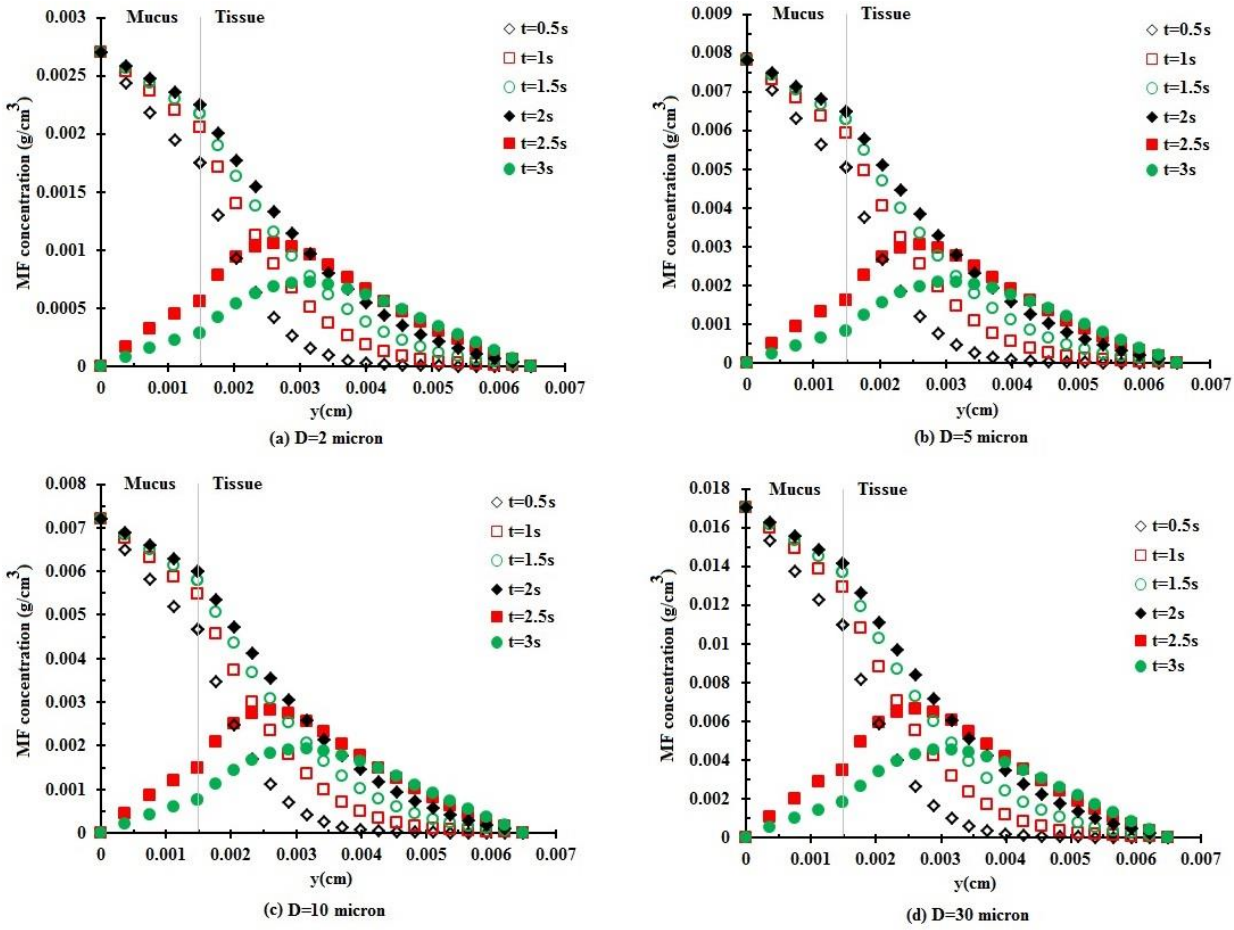

Figure 11. Concentration distribution in the AMTB system for Q=10L/min.

the mucus increases, and the drug penetrates the tissue. During this time, the medicine has not yet been spread in the whole of the tissue. At the end of the inhalation phase, i.e. at t=2 s, the drug is completely distributed in the mucus and tissues and reaches the maximum amount. It is also observed that over the inhalation phase, there is drug transfer from the mucus to the tissue. The highest initial concentration and the maximum peak value were observed for 30 μm particles. Previous studies [22] showed that such high concentrations in the respiratory system with the origin of destructive particles, such as influenza A virus, are met with a rapid response from the immune system.

For the 2, 5, 10, and 30 µm particles at the breathing rates of 5, 7.5, and 10 L/min, the time variation of the MF concentration at the mucus-tissue interface are shown in Figure 12. The figure shows that the peak value at the mucus-tissue interface occurs at the end of inhalation time because no particle deposition assumed during the exhalation. During the exhalation, the concentration values decrease over time. As noted before, an important parameter affecting drug concentration in mucus and tissue sides of interface is the mucus-tissue partition coefficient. For example, if a species is more soluble in mucus than in tissue at the mucus-tissue interface, its concentration will be higher in the mucus compared with the tissue. Figure 12 also shows that the highest MF concentration occurs during the inhalation phase and has a sharp drop when entering the exhalation mode.

The mass flux rate of the MF drug into the tissue is shown in Figure 13. It should be emphasized that at the start of inhalation the concentration of the medicine inside mucus and tissue layers is assumed to be zero. It is seen that for all cases, the maximum transient flux is obtained at t=0.5 s. Since the initial concentration is zero, it is observed that the flux into the tissue initially has the maximum value. It is also seen that the highest flux is obtained for the case (d). This is due to the higher initial concentration of 30 µm particles compared to the other sizes. It should be noted that inhalation of therapeutic aerosols to improve respiratory diseases has the profit of getting great local concentrations which results in a rapid of drug influence. Administration of biologically active compounds by inhalation has the extra advantage of enhancing the bioavailability of medicines with low oral bioavailability, which permits the application of a smaller dose and the reduction of systemic side effects [30].

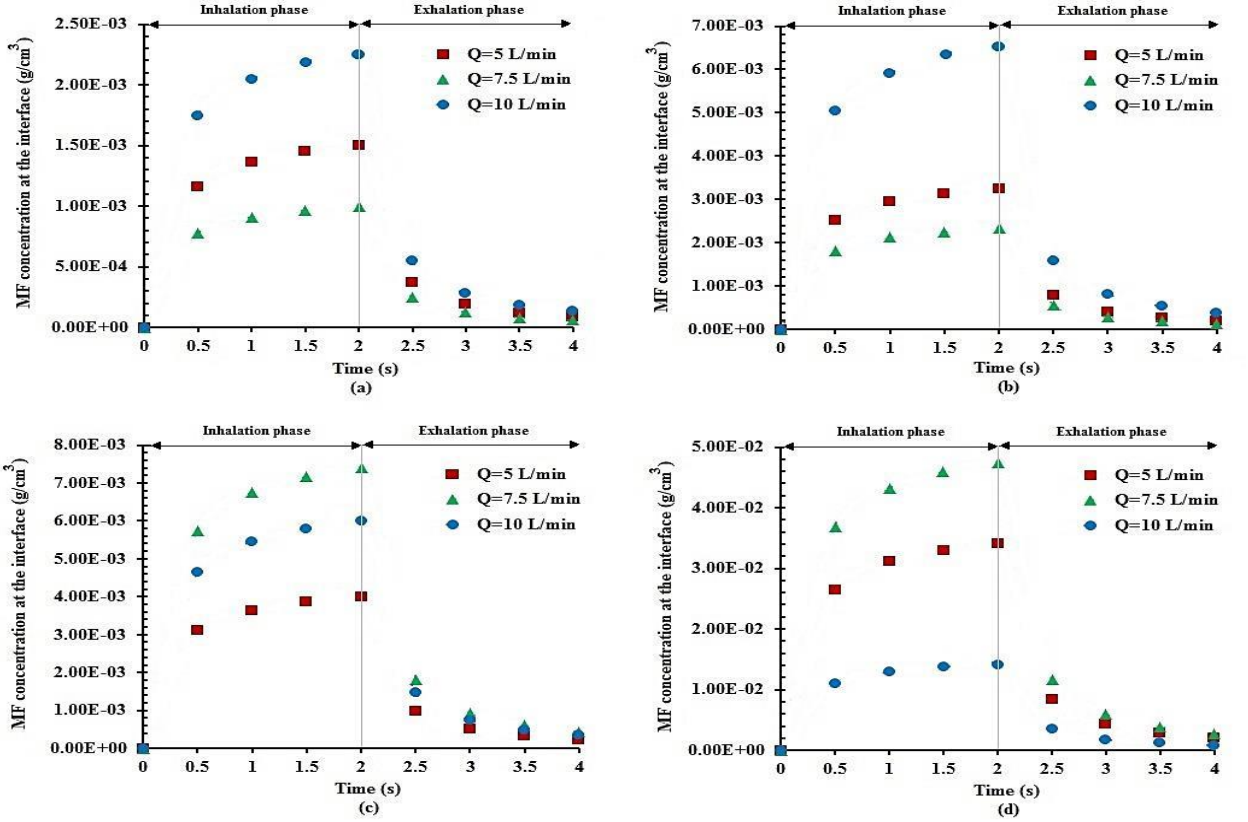

Figure 12. Time evolution of MF concentration at the mucus-tissue interface for (a) 2 µm, (b) 5 µm, (c) 10 µm, and (d) 30 µm particles.

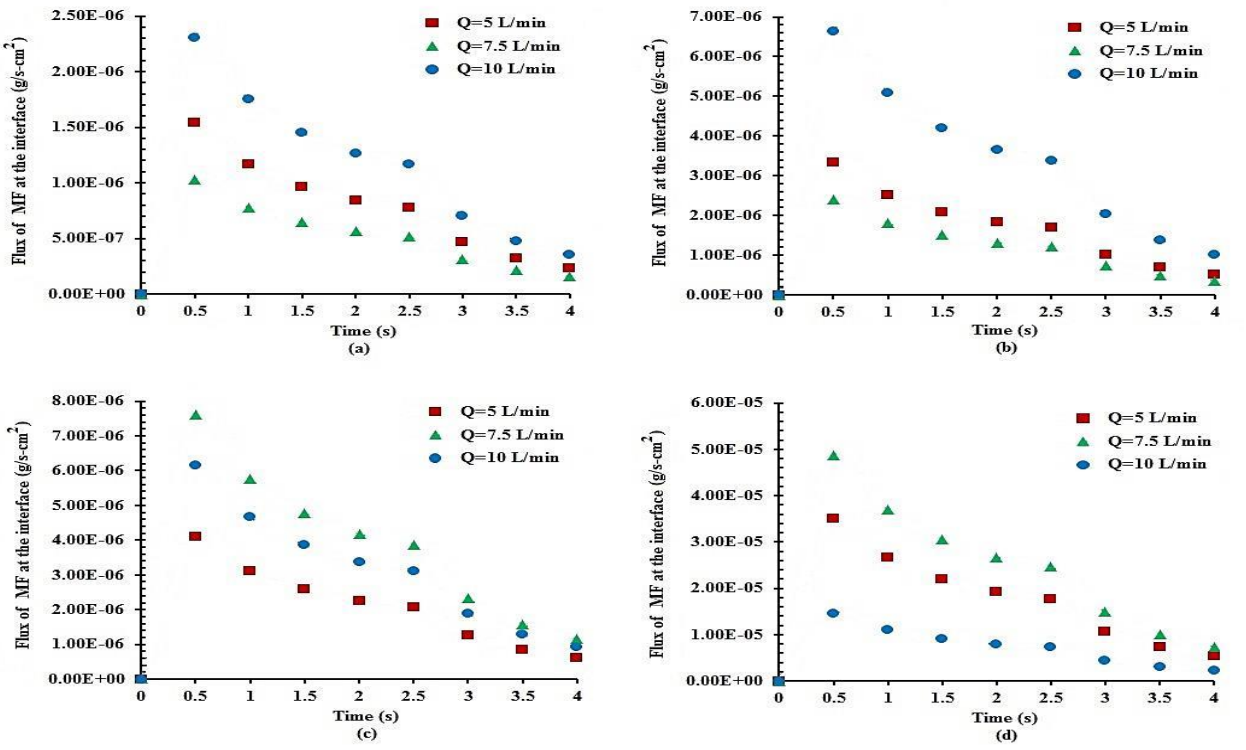

Figure 13. Flux of MF into the tissue for (a) 2 µm, (b) 5 µm, (c) 10 µm, and (d) 30 µm particles

Conclusion

While respiration through the nose is the natural condition, mouth breathing occurs on certain occasions, and in particular, during inhalation drug delivery. This study investigated the transient absorption of therapeutic drug particles in a multilayer system of the respiratory tract wall. For this purpose, a 3-D realistic respiratory airways model extending from oral to the end of the trachea was coupled to a 1-D diffusion model. Airflow was simulated by the CDF method, and a FORTRAN code was developed that implicitly solved the system of governing absorption equations. For the multilayer model considered, the results showed that the absorption process was strongly time-dependent. The simulation results were compared with the data reported in studies of Tian & Longest [27-28] good agreement was found. The results showed that during the inhalation time, the concentration of drugs increases while at the exhalation phase the concentration reduces. Also, the drug mass flux through the mucus-tissue interface and the drug concentration in the tissue decreased with time.

Nomenclature

C	slip correction factor
C_a	speices concentration in the air
C_m	speices concentration in the mucus
D_m	mucus diffusion coefficient
D_t	tissue diffusion coefficient
D_p	particle diameter
MF	Mometasone furoate
p	pressure
t	time
u_i	velocity of airflow
x_i	direction
St	Stokes number
U	mean axial fluid velocity
μ	dynamic viscosity
ρ	density
ρ_p	density of the particle
λ_{ba}	air − blood partition coefficien
λ_{bt}	blood − tissue partition coefficient
λ_{am}	air − mucus partition coefficient
λ_{tm}	tissue − mucus partition coefficient

References

[1] P. Koullapis, S. Kassinos, M.P. Bivolarova, A.K. Melikov, Particle deposition in a realistic geometry of the human conducting airways: Effects of inlet velocity profile, inhalation flow rate and electrostatic charge, Journal of Biomechanics, 49, 2201–2212, (2016).

[2] N.L. Phuong, K. Ito, Investigation of flow pattern in upper human airway including oral and nasal inhalation by PIV and CFD, Building and Environment, 94, 504-515, (2015).

[3] A. Naseri, S. Shaghaghian, O. Abouali, G. Ahmadi, Numerical investigation of transient transport and deposition of microparticles under unsteady inspiratory flow in human upper airways, Respiratory Physiology and Neurobiology, 244, 56-72, (2017).

[4] Y. Wang, Y. Zhao, J. Yao, Large eddy simulation of particle deposition and resuspension in turbulent duct flows, Advanced powder technology, 30, 656-671, (2019).

[5] V.K. Srivastav, A.R. Paul, A. Jain, Capturing the wall turbulence in CFD simulation of human respiratory tract, Mathematics and computers in simulation, 160(C), 23-38, (2019).

[6] Y. Hemmati, R. Rafee, Effects of the shape and height of artificial 2D roughness elements on deposition of nano and microparticles in the turbulent gas flow inside a horizontal channel, Journal of aerosol science, 122, 45-58, (2018).

[7] H. Mirzaee, R. Rafee, G. Ahmadi, Inertial impaction of particles on a circular cylinder for a wide range of Reynolds and P numbers: A comparative study, Journal of aerosol science, 135, 86-102, (2019).

[8] M.H. Hamedi Estakhrsar, R. Rafee, Effects of wavelength and number of bends on the performance of zigzag demisters with drainage channels, Applied mathematical modeling, 40 (2), 685-699, (2016).

[9] P. Zamankhan, G. Ahmadi, Z. Wang, P.K. Hopke, W.C. Su, Y.S. Cheng, D. Leonard, Airflow and Deposition of Nano-Particles in human Nasal Cavity, Aerosol science and technology, 40, 463-476, (2006).

[10] K.T. Shanley, P. Zamankhan, G. Ahmadi, P.K. Hopke, Y.S. Cheng, Numerical Simulations Investigating the Regional and Overall Deposition Efficiency of the Human Nasal Cavity, Inhalation toxicology, 20, 1093-1100, (2008).

[11] E. Ghahramani, O. Abouali, H. Emdad, G. Ahmadi, Numerical Analysis of Stochastic Dispersion of Micro-Particles in Turbulent Flows in A Realistic Model of Human Nasal/Upper Airway, Journal of aerosol science, 67, 188-206, (2014).

[12] P.F. Ghalati, E. Keshavarzian, O. Abouali, A. Faramarzi, T. Jiyuan, A. Shakibafard,

Numerical analysis of micro-and nano-particle deposition in a realistic human upper airway, Computers in biology and medicine, 42, 39–49, (2012).

[13] H. Nikookar, O. Abouali, M. Eghtesada, S. Sadrizadeh, G. Ahmadi, Enhancing drug delivery to human trachea through oral airway using magnetophoretic steering of microsphere carriers composed of aggregated superparamagnetic nanoparticles and nanomedicine: A numerical study, Journal of aerosol science, 127, 63–92, (2019).

[14] O. Abouali, E.E. Keshavarzian, P.F. Ghalati, A. Faramarzi, G. Ahmadi, M.H. Bagheri, Micro and Nanoparticle Deposition in Human Nasal Passage Pre and Post Virtual Maxillary Sinus Endoscopic Surgery, Respiratory physiology & neurobiology, 181, 335-345, (2010).

[15] A.A. Mofakham, G. Ahmadi, Particles dispersion and deposition in inhomogeneous turbulent flows using continuous random walk models, Physics of fluids, 31, 083301, (2019).

[16] E.M. Mina, G. Ghorbaniasl, C. Lacor, Study of nanoparticles deposition in a human upper airway model using a dynamic turbulent Schmidt number, AinShams engineer journal, 9 (4), (2017).

[17] K. Mohebbi, R. Rafee, F. Talebi, Effects of the rectangular groove dimensions on the thermal features of the turbulent Al2O3-water nanofluid flow in the grooved tubes, Journal of Heat and Mass Transfer Research, 2 (1), 59-70, (2015).

[18] R. Rafee, Entropy generation calculation for laminar fully developed forced flow and heat transfer of nanofluids inside annuli, Journal of Heat and Mass Transfer Research, 1 (1), 25-33, (2014).

[19] R. Tabe, R. Rafee, M.S. Valipour, G Ahmadi, Investigation of airflow at different activity conditions in a realistic model of human upper respiratory tract, Computer Methods in Biomechanics and Biomedical Engineering, (2020). doi: 10.1080/10255842.2020.1819256.

[20] M. Yousefi, O. Pourmehran, M. Gorji-Bandpy, K. Inthavong, L. Yeo, J. Tu, CFD simulation of aerosol delivery to a human lung via surface acoustic wave nebulization, Biomechanics and modeling in mechanobiology, 16(6), 2035-2050, (2017).

[21] Y. Shang, J. Dong, L. Tian, K. Inthavong, J. Tu, Detailed computational analysis of flow dynamics in an extended respiratory airway model, Clinical biomechanics, 61, 105–111, (2019).

[22] A. Haghnegahdar, J. Zhao, Y. Feng, Lung aerosol dynamics of airborne influenza A virus-laden droplets and the resultant immune system responses: An in silico study, Journal of aerosol science, 134, 34–55, (2019).

[23] F. Greifzu, C. Kratzsch, T. Forgber, F. Lindner, R. Schwarze, Assessment of particle-tracking models for dispersed particle-laden flows implemented in OpenFOAM and ANSYS FLUENT, Engineering Applications of Computational Fluid Mechanics, 10 (1), 30-43, (2016).

[24] J. Tu, K. Inthavong, G. Ahmadi, Computational Fluid and Particle Dynamics in the Human Respiratory System, Springer Dordrecht Heidelberg London, NewYork, (2013).

[25] E.A. Cohen Hubal, J.S Kimbell, P.S. Fedkiw, Incorporation of nasal-lining mass transfer resistance into acfd model for prediction of ozone dosimetry in the upper respiratory tract, Inhalation Toxicology, 8, 831–857, (1996).

[26] K. Keyhani, P.W. Scherer, M.M. Mozell, A numerical model of nasal odorant transport for the analysis of human olfaction, Journal Theoretical Biology, 186, 279–301, (1997).

[27] G. Tian, P.W. Longest, Transient Absorption of Inhaled Vapors into a Multilayer Mucus-Tissue-Blood System, Annals of Biomedical Engineering, 38(2), 517–536, (2010).

[28] G. Tian, P.W. Longest, Development of a CFD boundary condition to model transient vapor absorption in the respiratory airways, Journal of Biomechanical Engineering, 132, 051003–051013, (2010).

[29] G. Tian, Vapor transport and aerosol dynamics in the respiratory airways, PhD Thesis, Virginia Commonwealth University, (2011).

[30] A.J. Hickey, H.M. Mansour, Inhalation Aerosols, Physical and Biological Basis for Therapy, third edition, New York, CRC Press, (2019).

[31] ICRP, Human Respiratory Tract Model for Radiological Protection, Elsevier Science, New York, (1994).

[32] A. Rygg, M. Hindle, P.W. Longest, Linking Suspension Nasal Spray Drug Deposition Patterns to Pharmacokinetic Profiles: A Proof-of Concept Study Using Computational Fluid Dynamics, Journal of Pharmaceutical Sciences, 105, 1995-2004, (2016).

[33] Y. Cu, W.M. Saltzman, Mathematical modeling of molecular diffusion through mucus, Advanced Drug Delivery Reviews, 61(2), 101-114, (2009).

[34] J.S. Gulliver, Introduction to Chemical Transport in the Environment, Cambridge, UK University Press, (2007).
[35] S.C. George, A.L. Babb, M.E. Deffebach, M.P. Hlastala, Diffusion of nonelectrolytes in the canine trachea: Effect of thigh junction, Journal of Applied Physiology, 80, 1687-1695, (1996).
[36] M.P. Hlastala, H.T. Robertson, Complexity in Structure and Function of the Lung, Informa Health Care, (1998).
[37] J.C. Anderson, A.L. Babb, M.P. Hlastala, Modeling soluble gas exchange in the airways and alveoli, Annals of Biomedical Engineering, 31, 1402-1422, (2003).
[38] D.Y.H. Pui , F. Romay-Novas, B.Y.H. Liu, Experimental Study of Particle Deposition in Bends of Circular Cross Section, Aerosol Science and Technology, 7(3), 301-315, (1987).
[39] R. Talhout, A. Opperhuizen, J.G.C. van Amsterdam, Role of Acetaldehyde in Tobacco Smoke Addiction, European Neuropsychopharmacology, 17, 627–636, (2007).
[40] S. Nickel, C.G. Clerkin, M.A. Selo, C. Ehrhardt, Transport mechanisms at the pulmonary mucosa: Implications for drug delivery, Expert Opinion on Drug Delivery, 13(5), 667–690, (2016).
[41] M. Gumbleton, G. Al-Jayyoussi, A. Crandon-Lewis, D. Francombe, K. Kreitmeyr, C.J. Morris, M.W. Smith, Spatial expression and functionality of drug transporters in the intact lung: Objectives for further research, Advanced Drug Delivery Reviews, 63(1–2), 110–118, (2011).
[42] C. A. Ruge, J. Kirch, C.M. Lehr, Pulmonary drug delivery: From generating aerosols to overcoming biological barriers-therapeutic possibilities and technological challenges, Lancet Respiratory Medicine, 1(5), 402–413, (2013).
[43] M. Geiser, Update on macrophage clearance of inhaled microand nanoparticles, Journal of Aerosol Medicine and Pulmonary Drug Delivery, 23(4), 207–217, (2010).
[44] N.R. Labiris, M.B. Dolovich, Pulmonary drug delivery. Part I: Physiological factors affecting therapeutic effectiveness of aerosolized medications, British Journal of Clinical Pharmacology, 56(6), 588–599, (2003).
[45] M.B. Dolovich, Aerosols, In: P.J. Barnes, M.M. Grunstein, editors, Asthma, Philadelphia: Lippincott-Raven, 1349-65, (1997).